Scientia Iranica A (2016) 23(2), 535–547

SCIENTIA IRANICA

Sharif University of Technology
Scientia Iranica
Transactions A: Civil Engineering
www.scientiairanica.com

Topology and geometry optimization of single-layer domes utilizing CBO and ECBO

A. Kaveh[a,*] **and M. Rezaei**[b]

a. *Centre of Excellence for Fundamental Studies in Structural Engineering, Iran University of Science and Technology, Narmak, Tehran, P.O. Box 16846-13114, Iran.*
b. *Road, Building and Housing Research Center, Tehran, P.O. Box 1145-1696, Iran.*

Received 4 July 2015; received in revised form 20 September 2015; accepted 3 November 2015

KEYWORDS
Optimum structural design;
Enhanced colliding bodies optimization;
Ribbed dome;
Schwedler domes;
Nonlinear design.

Abstract. Dome structures are elegant and economical structures used for covering large areas. In this paper, an optimum topology design is performed using the Colliding Bodies Optimization (CBO) method and its enhanced version (ECBO). The Schwedler and ribbed domes are studied determining the optimum number of rings, the optimum number of joints in each ring, the optimum height of crown, and tubular sections of these domes. The minimum volume of each dome is taken as the objective function. A simple procedure is defined to determine the configurations of Schwedler and ribbed domes. This procedure includes calculation of the joint coordinates and element constructions. The design constraints are implemented according to the provision of LRFD-AISC. First, a comparative study for domes using different algorithms is carried out, and then the effect of choosing different number of joints in each ring on the optimal topology is investigated for Schwedler domes to verify the suitability of design procedure and to demonstrate effectiveness of the ECBO.

1. Introduction

Covering large areas without intermediate supports has always been a challenging task for structural engineers. Domes provide economical solution to this problem. The dome shape not only provides elegant appearance, but also offers one of the most efficient interior atmospheres for human residence, because air and energy circulation can be placed without obstruction. The basic parameters that define the geometry of a dome are the total number of rings and height of crown, once its diameter is specified. Consequently, optimum topological design of domes necessitates treatments of these parameters as design variables. The design constraints that are to be considered in the formulation of the design problem can be implemented according to one of the current design codes. In general, for optimum design of domes, the allowable cross-sections are selected from 37 standard steel pipe sections, as shown in Table 1. Other sections are rarely utilized as the members of domes. Load and Resistance Factor Design-American Institute of Steel Constitution (LRFD-AISC) is adopted in most of the research papers for design. Optimization methods can be divided in two general categories: (i) Mathematical programming methods that use approximation techniques to solve the optimization problem; and (ii) Meta-heuristic algorithms [1-3] that mimic some natural phenomena, including biology and evolution theory. Popular meta-heuristic algorithms are Particle Swarm Optimization (PSO) [3], Ant Colony Optimization (ACO) [4], Big Bang-Big Crunch (BB-BC) [5], Charged System Search (CSS) [6], Ray Optimization (RO) [7], and Dolphin Echolocation (DE) [8]. The

*. *Corresponding author. Tel: +98 21 77240104; Fax: +98 21 77240398*
E-mail address: alikaveh@iust.ac.ir (A. Kaveh)

Table 1. The allowable steel pipe sections taken from LRFD AISC.

	Type	Nominal diameter (in)	Weight per ft. (lb)	Area (in^2)	I (in^4)	S (in^3)	J (in^4)	Z (in^3)
1	ST	1/2	0.85	0.250	0.017	0.041	0.082	0.059
2	EST	1/2	1.09	0.320	0.020	0.048	0.096	0.072
3	ST	3/4	1.13	0.333	0.037	0.071	0.142	0.100
4	EST	3/4	1.47	0.433	0.045	0.085	0.170	0.125
5	ST	1	1.68	0.494	0.087	0.133	0.266	0.187
6	EST	1	2.17	0.639	0.106	0.161	0.322	0.233
7	ST	$1\frac{1}{4}$	2.27	0.669	0.195	0.235	0.470	0.324
8	ST	$1\frac{1}{2}$	2.72	0.799	0.310	0.326	0.652	0.448
9	EST	$1\frac{1}{4}$	3.00	0.881	0.242	0.291	0.582	0.414
10	EST	$1\frac{1}{2}$	3.63	1.07	0.666	0.561	1.122	0.761
11	ST	2	3.65	1.07	0.391	0.412	0.824	0.581
12	EST	2	5.02	1.48	0.868	0.731	1.462	1.02
13	ST	$2\frac{1}{2}$	5.79	1.70	1.53	1.06	2.12	1.45
14	ST	3	7.58	2.23	3.02	1.72	3.44	2.33
15	EST	$2\frac{1}{2}$	7.66	2.25	1.92	1.34	2.68	1.87
16	DEST	2	9.03	2.66	1.31	1.10	2.2	1.67
17	ST	$3\frac{1}{2}$	9.11	2.68	4.79	2.39	4.78	3.22
18	EST	3	10.25	3.02	3.89	2.23	4.46	3.08
19	ST	4	10.79	3.17	7.23	3.21	6.42	4.31
20	EST	$3\frac{1}{2}$	12.50	3.68	6.28	3.14	6.28	4.32
21	DEST	$2\frac{1}{2}$	13.69	4.03	2.87	2.00	4.00	3.04
22	ST	5	14.62	4.30	15.2	5.45	10.9	7.27
23	EST	4	14.98	4.41	9.61	4.27	8.54	5.85
24	DEST	3	18.58	5.47	5.99	3.42	6.84	5.12
25	ST	6	18.97	5.58	28.1	8.50	17.0	11.2
26	EST	5	20.78	6.11	20.7	7.43	14.86	10.1
27	DEST	4	27.54	8.10	15.3	6.79	13.58	9.97
28	ST	8	28.55	8.40	72.5	16.8	33.6	22.2
29	EST	6	28.57	8.40	40.5	12.2	24.4	16.6
30	DEST	5	38.59	11.3	33.6	12.1	24.2	17.5
31	ST	10	40.48	11.9	161	29.9	59.8	39.4
32	EST	8	43.39	12.8	106	24.5	49.0	33.0
33	ST	12	49.56	14.6	279	43.8	87.6	57.4
34	DEST	6	53.16	15.6	66.3	20.0	40.0	28.9
35	EST	10	54.74	16.1	212	39.4	78.8	52.6
36	EST	12	65.42	19.2	362	56.7	113.4	75.1
37	DEST	8	72.42	21.3	162	37.6	75.2	52.8

Colliding Bodies Optimization was recently introduced for design of structures with continuous and discrete variables [9]. The CBO algorithm reproduces the laws of collision between bodies. Each Colliding Body (CB) is considered to be an object with specified mass and velocity before collision; after collision, each CB moves to a new position with new velocity [10]. The design optimization of geometrically nonlinear geodesic domes is carried out where the developed design algorithm determines the optimum height of the crown as well as the optimum tubular steel sections for its members using genetic algorithm [11]. In this paper, optimum topology design of linear elastic geodesic domes is presented. The design algorithm determines the optimum number of rings, the optimum height of crown, and tubular sections for the geodesic domes. The optimum topology design algorithm based on the hybrid Big Bang-Big Crunch optimization method is presented for the Schwedler and Ribbed domes in Kaveh and Talatahari [12]. A comparative study is carried out for the optimum design of different types of single-layer latticed domes in Kaveh and Talatahari [13]. In Kaveh and Talatahari [14], the optimum geometry and topology design of geodesic domes is obtained by using Charged System Search (CSS). Recently, Gonçalves et al. [15] presented search group algorithm, and Mirjalili developed the ant lion optimizer [16]. Applications to some real-life problems can be found in the work of [17-19].

The present paper is structured as follows: Section 2 consists of optimum design of ribbed and Schwedler domes according to LRFD domes. Section 3 recalls the laws of collision between two bodies. Section 4 illustrates the configuration of domes. Comparative study is performed for ribbed and Schwedler domes using CBO algorithm, and then topology optimization of Schwedler dome with different number of nodes in each ring is investigated in Section 5. Finally, Section 6 concludes the main findings of this study.

2. Optimum design problem of ribbed and Schwedler domes according to LRFD

Optimal design of Schwedler and ribbed domes consists of finding optimal cross-sections for elements, optimal height for the crown, optimal number of the nodes in each ring, and the optimum number of rings under the determined loading conditions. The allowable cross-sections are 37 steel pipe sections, as shown in Table 1, which are standard sections. In this table, the abbreviations ST, EST, and DEST stand for standard weight, extra strong, and double-extra strong, respectively. These sections are taken from LRFD-AISC [20] which is also utilized as the code of practice. The process of the optimum design of the structures of a dome can be summarized as:

$$\text{Find} \quad X = [x_1, x_2, ..., x_{ng}], h, Nr \tag{1}$$

$$x_i \in \{d_1, d_2, ..., d_{ng}\}$$

$$h_i \in \{h_{\min}, h_{\min} + h^*, ..., h_{\max}\}$$

$$\text{To minimize} \quad V(x) = \sum_{i=1}^{nm} x_i . l_i$$

subjected to the following constraints:
Displacement constraints:

$$\delta_i \leq \delta_i^{\max} \qquad i = 1, 2, ..., nn. \tag{2}$$

Interaction formula constraints:

$$\frac{P_u}{2\phi_c P_n} + \left(\frac{M_{ux}}{\phi_b M_{nx}} + \frac{M_{uy}}{\phi_b M_{ny}}\right) \leq$$

$$\text{for } \frac{P_u}{\phi_c P_n} < 0.2, \tag{3}$$

$$\frac{P_u}{\phi_c P_n} + \frac{8}{9}\left(\frac{M_{ux}}{\phi_b M_{nx}} + \frac{M_{uy}}{\phi_b M_{ny}}\right) \leq 1$$

$$\text{for } \frac{P_u}{\phi_c P_n} \geq 0.2, \tag{4}$$

where X is the vector containing the design variables of the elements; h is the variable of the crown height; Nr is the total number of rings; d_j is the jth allowable discrete value for the design variables; $h_{\min}$, $h_{\max}$, and h^* are the permitted minimum, maximum and increased amounts of the crown height, which in this paper are taken as $D/20$, $D/2$, and 0.25 m, respectively, in which D is the diameter of the dome; ng is the number of design variables or the number of groups; $V(x)$ is the volume of the structure; l_i is the length of member i; δ_i is the displacement of node i; $\delta_{\max}$ is the permitted displacement for the ith node; nn is the total number of nodes; ϕ_c is the resistance factor ($\phi_c = 0.9$ for tension, $\phi_c = 0.85$ for compression); ϕ_b is the flexural resistance reduction factor ($\phi_b = 0.9$); M_{ux} and M_{uy} are the required flexural strengths in the x and y directions, respectively; M_{nx} and M_{ny} are the nominal flexural strengths in the x and y directions, respectively; P_u is the required strength; and P_n denotes the nominal axial strength, which is computed as:

$$P_n = A_g F_{cr}, \tag{5}$$

where A_g is the gross area of a member; and F_{cr} is calculated as follows:

$$F_{cr} = (0.658^{\lambda_c^2}).f_y \quad \text{for} \quad \lambda_c \leq 1.5, \tag{6}$$

$$F_{cr} = \left(\frac{0.877}{\lambda_c^2}\right).f_y \quad \text{for} \quad \lambda_c > 1.5. \tag{7}$$

Here, f_y is the specified yield stress; and λ_c is obtained from:

$$\lambda_c = \frac{kl}{\pi r}\sqrt{\frac{f_y}{E}}, \tag{8}$$

where k is the effective length factor taken as 1; l is the length of a dome member; r is the governing radius of gyration about the axis of buckling; and E is the modulus of elasticity. In Eq. (9), V_u is the factored service load shear; V_n is the nominal strength in shear; and φ_v represents the resistance factor for shear ($\varphi_v = 0.9$).

$$V_u \leq \varphi_v V_n. \tag{9}$$

3. The CBO and ECBO algorithm

This section introduces the recently developed meta-heuristic Colliding Bodies Optimization (CBO) algorithm and its enhanced version based on the work of Kaveh and Mahdavi [9], Kaveh [21], and Kaveh and Ilchi Ghazaan [22,23], respectively.

3.1. Colliding bodies optimization

The CBO mimics the one-dimensional collision law between bodies. In CBO, each solution candidate X_i containing a number of variables (i.e., $X_i = \{x_{i,j}\}$) is considered to be a Colliding Body (CB). The massed objects composed of two main groups, equally; namely stationary and moving objects, where the moving objects move to follow stationary objects and a collision occurs between pairs of objects. This is done for two purposes: (i) to improve the positions of moving objects; and (ii) to push stationary objects towards better positions. After the collision, the new positions of colliding bodies are updated based on the new velocity by using the collision laws; and the lighter and heavier CBs move sharply and slowly, respectively (Figure 1).

The pseudo-code for the CBO algorithm can be summarized as follows:

Step 1: *Initialization.* The initial positions of CBs are determined with random initialization of a population of individuals in the search space:

$$x_i^0 = x_{\min} + \text{rand}(x_{\max} - x_{\min}), \quad i = 1, 2, 3, ..., n, \tag{10}$$

where x_i^0 determines the initial design vector of the ith CBs; $x_{\max}$ and $x_{\min}$ are the minimum and the maximum allowable values for the variables; rand is a random number in the interval [0, 1]; and n is the number of CBs.

Step 2: The magnitude of the body mass for each CB is defined as:

$$m_k = \frac{\frac{1}{fit(k)}}{\sum_{i=1}^{n} \frac{1}{fit(i)}}, \quad k = 1, 2, ..., n, \tag{11}$$

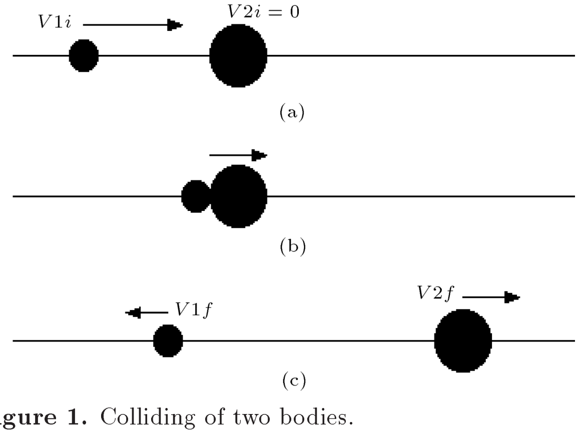

Figure 1. Colliding of two bodies.

where $fit(i)$ represents the fitness value of the agent i; n is the population size. It is clear that a CB with a good value exerts a larger mass than the bad one. In maximization problems, the term $(1/fit)$ is replaced by $fit(i)$.

Step 3: *Mating of bodies.* CBs costs are sorted in ascending order based on the value of cost function. The sorted CBs are divided equally into two groups:

- The lower half of CBs (stationary CBs) includes good agents that are stationary and velocity of these bodies before collision is zero. Thus:

$$v_i = 0, \quad i = 1, ..., \frac{n}{2} \tag{12}$$

- The upper half of CBs (moving CBs) includes agents that move toward the lower half. Then (see Figure 1), the better and worse CBs, i.e. agents with upper fitness value of each group, will collide with each other. The change of the body position represents the velocity of these bodies before collision as:

$$v_i = x_{i-\frac{n}{2}} - x_i, \quad i = \frac{n}{2} + 1, ..., n, \tag{13}$$

where v_i and x_i are the velocity and position vectors of the ith CB in this group, respectively, and $x_{i-n/2}$ is the ith CB pair position of x_i in the previous group.

Step 4: *Updating velocities.* After the collision, the velocity of bodies in each group is evaluated using Eqs. (13) and (14) and the velocity before collision. The velocity of each moving CB after the collision is:

$$v_i' = \frac{\left(m_i - \varepsilon m_{i-\frac{n}{2}}\right) v_i}{m_i + m_{i-\frac{n}{2}}} \quad i = \frac{n}{2} + 1, \frac{n}{2} + 2, ..., n, \tag{14}$$

where v and v_i^0 are the velocities of the ith moving CB before and after the collision, respectively; m_i is mass of the ith CB; $m_{i-n/2}$ is mass of the ith CB pair. Also, the velocity of each stationary CB after the collision is:

$$v_i' = \frac{\left(m_{i+\frac{n}{2}} + \varepsilon m_{i-\frac{n}{2}}\right) v_{i+\frac{n}{2}}}{m_i + n_{i+\frac{n}{2}}} \quad i = 1, 2, ..., \frac{n}{2}, \tag{15}$$

where $v_{i+\frac{n}{2}}$ and v_i^0 are the velocities of the ith moving CB pair before the collision and the ith stationary CB after the collision, respectively; m_i is mass of the ith CB; $m_{i+\frac{n}{2}}$ is mass of the ith moving CB pair; ε is the Coefficient Of Restitution (COR), which is defined as the ratio of the separation velocity of two agents after collision to the approach velocity of two agents before collision. For most of the real objects, ε is between 0 and 1. Therefore, to control exploration and exploitation rates, COR decreases linearly from unity to zero and ε is defined as:

$$\varepsilon = 1 - \frac{\text{iter}}{\text{iter}_{\max}} \tag{16}$$

Step 5: *Updating positions.* New positions of CBs are evaluated using the generated velocities after the collision in position of stationary CBs. The new position of each moving CB is:

$$x_i^{\text{new}} = x_{i-\frac{n}{2}} + \text{rand } 0v_i', \quad i = \frac{n}{2} + 1, ..., n, \tag{17}$$

where $x_i^{\text{new}'}$ and v_i' are the new position and the velocity after the collision of the ith moving CB, respectively; and $x_{i-n/2}$ is the old position of ith stationary CB pair. Also, the new position of each stationary CB is:

$$x_i^{\text{new}} = x_i + \text{rand } 0v_i', \quad i = 1, 2, ..., \frac{n}{2}, \tag{18}$$

where x_i^{new}, x_i, and v_i^0 are the new position, old position, and the velocity after the collision of the ith stationary CB, respectively. Rand is a random vector uniformly distributed in the Range (1,1).

Step 6: *Terminating criterion.* The optimization is repeated from Step 2 until a termination criterion, as the maximum number of iterations, is satisfied.

Apart from the efficiency of the CBO algorithm, which is illustrated in the next section through numerical examples, the independence of the algorithm from internal parameters is one of the main advantages of the CBO algorithm.

3.2. Discrete CBO algorithm

In this paper, a simple method is employed to solve discrete problems by using a continuous algorithm. This method utilizes a rounding function which changes the continuous value of a result to the nearest discrete value, as:

$$x_{\text{discrete}}^{\text{new}} = Fix(x_{\text{continuous}}^{\text{new}}), \tag{19}$$

where $Fix(X)$ is a function which rounds each element of X to the nearest permissible discrete value.

3.3. Enhanced colliding bodies optimization

A modified version of the CBO is Enhanced Colliding Bodies Optimization, which improves the CBO to get more reliable solutions. The introduction of memory can increase the convergence speed of ECBO with respect to standard CBO. Furthermore, changing some components of colliding bodies will help ECBO to escape from local optima. In short, in the Enhanced Colliding Bodies Optimization (ECBO), a memory that saves a number of historically best CBs is utilized to improve the performance of the CBO and reduce the computational cost. Furthermore, ECBO changes some components of CBs, randomly, to prevent premature convergence. The steps added to the standard CBO are as follow:

Added step 1: *Saving.* This step is put after Step 2 of standard CBO and considers a memory which saves some historically best CB vectors and their related mass and objective function values improve the performance of the algorithm without increasing the computational time, [22,23]. Here, a Colliding Memory (CM) is utilized to save a number of the best-so-far solutions. Therefore, at this step, the solution vectors saved in CM are added to the population, and the same numbers of current worst CBs are deleted. Finally, CBs are sorted according to their masses in a decreasing order.

Added step 2: *Escape from local optima.* This step is put after Step 7 of standard CBO. Meta-heuristic algorithms should have the ability to escape from the trap when agents get close to a local optimum. In ECBO, a parameter like Pro within (0, 1) is introduced and it is specified to determine whether a component of each CB must be changed or not. For each colliding body, Pro is compared with $rn_i (i = 1, 2, ..., n)$ which is a random number uniformly distributed within (0, 1). If $rn_i < Pro$, one dimension of the ith CB is selected randomly and its value is regenerated as follows:

$$x_{ij} = x_{j,\min} + \text{random}.(x_{j,\max} - x_{j,\min}), \tag{20}$$

where x_{ij} is the jth variable of the ith CB. $x_{j,\min}$ and $x_{j,\max}$, respectively, are the lower and upper bounds of the jth variable. In order to protect the structures of CBs, only one dimension is changed. This mechanism provides opportunities for the CBs to move all over the search space thus providing better diversity.

4. Configuration of Schwedler and ribbed domes

The configuration of a Schwedler dome is shown in Figure 2. This dome consists of meridional ribs connected together by a number of horizontal polygonal rings. To stiffen the resulting structure, each trapezium formed by intersecting meridional ribs with horizontal rings is subdivided into two triangles by introducing a diagonal member. The number of nodes in each ring for the

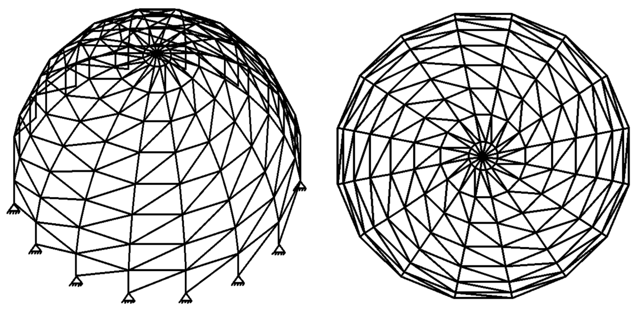

(a) Plan view (b) 3D view

Figure 2. The Schwedler dome.

Schwedler domes is considered constant and it is equal to 10 at the first stage. The distances between the rings in the dome on the meridian line are generally of equal length. The structural data for the geometry of this form of the Schwedler domes is a function of the diameter of the dome (D), the total number of rings (Nr), and the height of the crown (h). The total number of rings can be selected as 3, 4, or 5. The top joint at the crown is numbered as the first joint, as shown in Figure 2(a) (joint number 1), which is located in the center of the coordinate system in $x-y$ plane. The coordinates of other joints in each ring are obtained as:

$$\begin{cases} x_i = \frac{D}{2Nr}\cos\left(\frac{360}{4n_i}\left(i-\sum_{j=1}^{i-1}4n_j-1\right)\right) \\ z_i = \sqrt{\left(R^2-\frac{n_i^2D^2}{4Nr^2}\right)}-(R-h) \\ y_i = \frac{D}{2Nr}\sin\left(\frac{360}{4n_i}\left(i-\sum_{j=1}^{i-1}4n_j-1\right)\right) \end{cases} \tag{21}$$

where n_i is the number of rings corresponding to the node i; $R=(D^2+4h^2)/(8h)$, where R is the radius of the hemisphere as shown in Figure 2(b). The member of grouping is determined in a way that rib members between each consecutive pair of rings belong to one group, diagonal members belong to one group, and the members on each ring form another group. Therefore, the total number of groups is equal to $(3Nr-2)$. Figure 3 shows the number of groups corresponding to rib, diagonal, and ring members. The configuration of elements contains determining the start and end nodes of each element. For the first group, the start node for all elements is the joint number 1 and the end nodes are those on the first ring.

A dome without the diagonal members is called the ribbed dome, as shown in Figure 4. For these

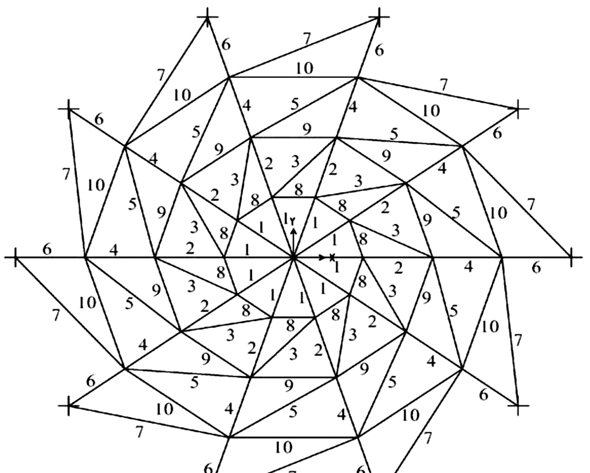

Figure 3. The Schwedler dome with the related member grouping.

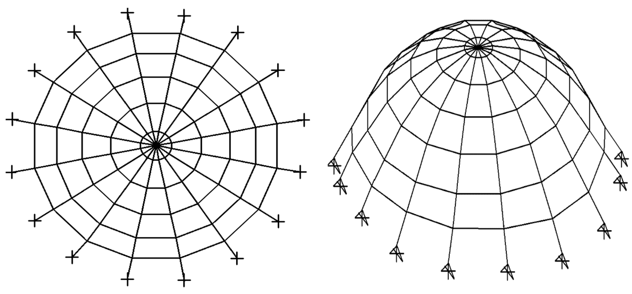

(a) Plan view (b) 3D view

Figure 4. The ribbed dome.

domes, Eqs. (19) and (20) are also valid to determine the joint coordinates and the ring member constructions. However, the rib members are assigned using the following relationship:

$$\begin{cases} I = 10*(n_i-1)+j+1 \\ J = 10*(n_i)+j+1 \end{cases} \qquad n_i = 1,2,...,Nr-1 \tag{22}$$

5. Results and discussion

In this section, two common domes are optimized utilizing the CBO and ECBO. Both ribbed and Schwedler domes have common configurations, which are widely used to cover large areas. Since a ribbed dome has less number of elements than a Schwedler dome, it will be interesting to compare their performance and optimum volumes, element sections, and their heights, when these domes are subjected to three different forms of equipment loading. Another reason for choosing these types of domes is the diagonal members in topology of the Schwedler domes in contrary to the ribbed domes.

The modulus of elasticity for the steel is taken as 205 kN/mm^2. The limitations imposed on the joint displacements are 28 mm in the z direction and 33 mm in the x and y directions for the 1st, 2nd, and 3rd nodes, respectively (Table 2).

The behavior of domes is nonlinear due to change of geometry under external loads. This is due to the imperfections arising either from the manufacturing process and/or from the construction of the structure. Furthermore, they are sometimes subjected to equipment loading concentrated at the crown in addition to uniform gravity loading. In the further step of this study, the domes are subjected to equipment loading. In order to show the effect of geometric nonlinearity on the behavior of domes, linear and nonlinear Z-displacements of joint 1 of the ribbed dome obtained from CBO algorithm are calculated under different concentrated loads. The linear analysis is performed by the commercial structural analysis program SAP2000v14 for comparison with the nonlinear analysis. It is apparent from Table 3 that under 500 kN downward load, nonlinear displacement is 12.94% more

Table 2. Displacement restrictions of single-layer ribbed and Schwedler domes.

	Displacement limitations (mm)					
	x direction		y direction		z direction	
Joint no	Upper bound	Lower bound	Upper bound	Lower bound	Upper bound	Lower bound
1	–	–	–	–	28	-28
2	33	-33	33	-33	28	-28
3	33	-33	33	-33	28	-28

Table 3. Z-displacement of joint 1 of ribbed dome with four rings obtained by the linear analysis using SAP200 v14 and nonlinear analysis by the routine developed in this work.

Load (kN)	Z-displacements of joint 1 obtained by carrying out the linear analysis using SAP2000 v14 (mm)	Z-displacements of joint 1 obtained by carrying out the nonlinear analysis developed in this work (mm)
0	0	0
100	13.63	14.27
200	14.72	16.63
300	17.18	19.09
400	19.63	21.63
500	22.09	24.95

than the linear displacement for ribbed dome with four rings.

5.1. Optimum design of the domes obtained by different methods

The diameter of the considered dome is selected as 40 m. The dome is subjected to equipment loading at its crown. The three loading conditions are as:

Case 1. The vertical downward load of 500 kN;

Case 2. The two horizontal loads of 100 kN in the x and y directions;

Case 3. The vertical downward load of 500 kN and two horizontal loads of 100 kN in the x and y directions.

Tables 4 and 5 present the results for the ribbed and Schwedler domes. The volume of dome structures can be considered a function of the average cross-sectional area of the elements ($\bar{A}$) and the sum of the element lengths written as:

$$V(X) = \bar{A}.\sum_{i=1}^{nm} l_i. \tag{23}$$

In all cases, both domes have approximately the same optimal height; however, because of having less number of elements, the ribbed dome has smaller value for the sum of the element lengths than that of the Schwedler dome.

When comparing the optimum sections for these two types of domes, it can be shown that the rib members in the ribbed dome have much stronger sections than the rings elements, while almost all members in the Schwedler dome have near cross-section areas. It can be shown that the rib members in the ribbed dome have much heavier sections than the rings elements, while almost all members in the Schwedler dome are not so much different. In other words, the results show that for providing lateral stiffness in the ribbed domes, all rib members should have very strong sections, and A has a very large value, whereas the Schwedler dome has small area sections because of having diagonal elements which provide the necessary lateral stiffness against the lateral external loadings. In short, the Schwedler dome has better performance against the external lateral forces and has smaller volume.

Because of the existence of only lateral forces in Case 2 loading, the angles of elements with the horizontal line in the optimum design should have the least value; therefore, the domes have the minimum allowable standard heights.

When Case 1 and Case 2 loading conditions are applied to the domes, for maintaining stability, the height of the ribbed dome is obtained smaller. On the contrary, for Schwedler domes, because of having more diagonal and ribbed members, the height is obtained bigger than that for the ribbed dome, and it is more stable.

Another observation is that the performance of ECBO is better than that of the CBO. ECBO finds

Table 4. Optimum design of the ribbed domes.

Group number	Optimum section (designations)					
	Case 1		Case 2		Case 3	
	(CBO)	(ECBO)	(CBO)	(ECBO)	(CBO)	(ECBO)
1	PIPST (8)	PIPST(8)	PIPST (8)	PIPPST(8)	PIPST (12)	PIPEST(12)
2	PIPST (5)	PIPST(5)	PIPST (8)	PIPST(8)	PIPST (12)	PIPEST(12)
3	PIPST (5)	PIPST(5)	PIPST (10)	PIPST(10)	PIPST (10)	PIPEST(10)
4	PIPST (8)	PIPST(8)	PIPST (1/2)	PIPST(1/2)	PIPST (8)	PIPST(10)
5	PIPST (5)	PIPST(5)	PIPST (1 1/4)	PIPST(1 1/4)	PIPST (8)	PIPEST(6)
Height (m)	13.25	13.00	2.00	2.00	7.25	7.25
Max. displacement (cm)	2.85	2.89	2.20	2.20	3.00	3.20
Max. strength ratio	0.80	0.82	0.60	0.60	0.82	0.79
Volume (m^3)	1.33	1.32	1.16	1.01	2.57	2.51
$\sum l_I$ (m)	375.92	374.11	324.90	324.90	340.20	340.20
$\bar{A}$(cm^2)	35.37	35.28	39.39	39.39	75.54	73.78

PIPST, PIPEST, and PIPDEST stand for standard weight, extra strong, and double-extra strong, respectively.

Table 5. Optimum design of the Schwedler domes.

Group number	Optimum section (designations)					
	Case 1		Case 2		Case 3	
	(CBO)	(ECBO)	(CBO)	(ECBO)	(CBO)	(ECBO)
1	PIPST (10)	PIPST(8)	PIPST (3)	PIPPST(8)	PIPST (10)	PIPEST(10)
2	PIPST (5)	PIPST(5)	PIPST (3)	PIPST(8)	PIPST (4)	PIPEST(4)
3	PIPST (2)	PIPST(1 1/2)	PIPST (2 1/2)	PIPST(10)	PIPST (6)	PIPEST(6)
4	PIPST (4)	PIPST(4)	PIPST (3)	PIPST(1/2)	PIPST (4)	PIPST(4)
5	PIPST (2)	PIPST(1 1/2)	PIPST (3 1/2)	PIPST(1 1/4)	PIPST (5)	PIPEST(5)
6	PIPST (10)	PIPST (8)	PIPST (2 1/2)	PIPST (2)	PIPST (8)	PIPST (8)
7	PIPST (2)	PIPST (5)	PIPST (2 1/2)	PIPST (2)	PIPST (5)	PIPST (5)
Height (m)	11.50	11.25	2.00	2.00	10.25	7.25
Max. displacement (cm)	3.10	3.20	1.86	1.84	3.18	3.10
Max. strength ratio	0.76	0.79	0.94	0.94	0.94	0.96
Volume (m^3)	1.38	1.34	0.73	0.71	2.02	2.01
$\sum l_I$ (m)	599.24	596.47	534.16	535.16	585.95	583.46
$\bar{A}$ (cm^2)	23.02	22.46	13.64	13.25	34.47	31.45

better results for all cases. As an example, volumes of Schwedler dome under Case 2 loading are obtained 0.71 and 0.73 for ECBO and CBO, respectively. This shows that ECBO has designed 2.7% lighter structure than CBO. Also for the ribbed dome under loading Case 1, the volumes are obtained 1.31 and 1.33 for ECBO and CBO, respectively, indicating that ECBO has obtained a lighter structure than CBO. To sum up, the ECBO algorithm is a robust method for optimum design of domes, having better performance than its standard version.

Figure 5 shows the convergence histories for the CBO and ECBO algorithms. This figure shows that

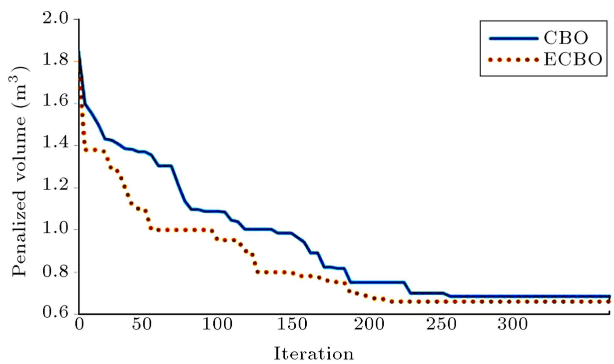

Figure 5. Optimization history of the Schwedler dome with 3 rings.

Table 6. Geometry and topology optimization of Schwedler domes with four rings using colliding bodies method.

Group number	$Nn = 6$	$Nn = 7$	$Nn = 8$	$Nn = 9$	$Nn = 10$
1	PIPST (10)	PIPST (10)	PIPST (10)	PIPST (10)	PIPST (10)
2	PIPST (8)	PIPST (8)	PIPST (8)	PIPST (8)	PIPST (8)
3	PIPST (8)	PIPST (8)	PIPST (8)	PIPST (8)	PIPST (8)
4	PIPST (5)	PIPST (5)	PIPST (5)	PIPST (5)	PIPST (5)
5	PIPST (2 1/2)	PIPST (2 1/2)	PIPST (2 1/2)	PIPST (2 1/2)	PIPST (2 1/2)
6	PIPST (5)	PIPST (5)	PIPST (4)	PIPST (3)	PIPST (3 1/2)
7	PIPST (2)	PIPST (1 1/2)	PIPST (1 1/2)	PIPST (1 1/2)	PIPST (1 1/2)
8	PIPST (8)	PIPST (8)	PIPST (8)	PIPST (8)	PIPST (8)
9	PIPST (5)	PIPST (5)	PIPST (4)	PIPST (4)	PIPST (4)
10	PIPST (4)	PIPST (4)	PIPST (4)	PIPST (4)	PIPST (3 1/2)
Optimum height (m)	6.00	5.50	5.00	4.50	4.25
Max. displacement (cm)	2.76	2.59	2.70	2.79	2.71
Max. strength ratio	91.85	80.61	72.33	92.89	72.17
Volume	0.8936	0.9619	0.9777	1.0438	1.08
$\sum l_I$ (m)	308.97	329.05	348.04	366.33	385.71
$\bar{x}$ (cm^2)	36.30	36.12	34.52	34.43	33.89

the design found by ECBO is lighter than that found by CBO at the same number of analyses. It can be seen that the convergence rate of the ECBO algorithm is better than that of the CBO.

5.2. Topology and geometry optimization of Schwedler domes with different number of nodes in each ring

In this section, the dome described in the previous section is optimized using the CBO algorithm while the number of rings (Nr) and the number of nodes in each ring (Nn) are defined as the design variables in our program. However, in order to investigate the effect of Nr and Nn on the optimum design, here, we consider all possible conditions for these design variables. The dome is considered to be subjected to equipment loading equal to 1000 kN, as shown in Figure 6. The modulus of elasticity for the steel is taken to be 205 kN/mm^2. The diameter of the dome is selected as 20 m. The limitations imposed on the joint displacements are according to Table 3. Nr and Nn determine the number of elements and the height of dome alters the length of elements to cause change in the sum of the element lengths. Tables 6, 7, and 8 present the optimal designs for the Schwedler dome with different number of nodes in each ring that is obtained by the CBO algorithm. Tables 6, 7, and 8 are related to domes with Nr being 3, 4, and 5, respectively. From these tables, it can be observed that a dome with small number of elements (Nn) tends to select the greater height. When Nn increases, almost in all the tables, the height of the domes decreases. For a dome with small Nn, having a large height helps the dome to prevent instability. Also it is clear that for Schwedler dome, the optimum volume is attained by 3 rings with 8 nodes on each ring, as shown in Figure 7. As a result, the selected sections for the elements in a dome with a small Nn are stronger than those of a dome with a larger value for Nn. This means that though a dome with small Nn has a small value for the sum of the element lengths, its average cross-sectional

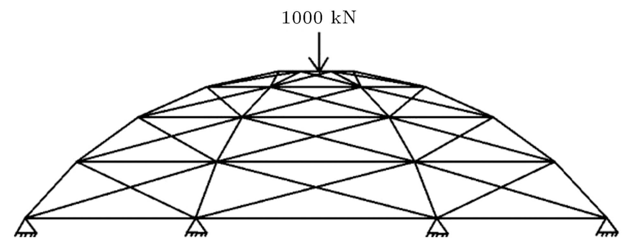

Figure 6. The Schwedler dome under equipment loading distributed in the first ring.

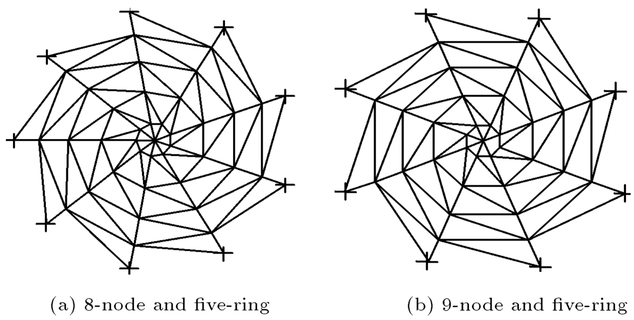

Figure 7. A 20 meter span Schwedler domes plan view with different number of nodes in each ring.

Table 7. Geometry and topology optimization of Schwedler domes with 5 rings using CBO.

Group number	$Nn = 6$	$Nn = 7$	$Nn = 8$	$Nn = 9$	$Nn = 10$
1	PIPST (10)	PIPST (10)	PIPST (10)	PIPST (10)	PIPST (10)
2	PIPST (8)	PIPST (8)	PIPST (8)	PIPST (8)	PIPST (8)
3	PIPST (8)	PIPST (8)	PIPST (8)	PIPST (8)	PIPST (8)
4	PIPST (5)	PIPST (5)	PIPST (5)	PIPST (5)	PIPST (4)
5	PIPST (2 1/2)	PIPST (2 1/2)	PIPST (2 1/2)	PIPST (2 1/2)	PIPST (2 1/2)
6	PIPST (5)	PIPST (5)	PIPST (3 1/2)	PIPST (3 1/2)	PIPST (3)
7	PIPST (2)	PIPST (2)	PIPST (2)	PIPST (1 1/2)	PIPST (1 1/2)
8	PIPST (5)	PIPST (4)	PIPST (3 1/2)	PIPST (3 1/2)	PIPST (3)
9	PIPST (1 1/2)	PIPST (1 1/2)	PIPST (1 1/2)	PIPST (1 1/2)	PIPST (1 1/2)
10	PIPST (5)	PIPST (4)	PIPST (4)	PIPST (4)	PIPST (4)
11	PIPST (6)	PIPST (4)	PIPST (4)	PIPST (4)	PIPST (4)
12	PIPST (5)	PIPST (4)	PIPST (4)	PIPST (3 1/2)	PIPST (3 1/2)
13	PIPST (5)	PIPST (4)	PIPST (4)	PIPST (3 1/2)	PIPST (3 1/2)
Height (m)	6.50	6.00	5.50	5.00	5.50
Max. displacement (cm)	2.71	2.80	2.79	2.79	2.75
Max. strength ratio	96.02	92.11	96.87	91.51	86.37
Volume	0.9114	0.8409	0.8682	0.8856	0.9117
$\sum l_I$ (m)	353.17	370.62	386.50	401.32	419.83
$\bar{x}$ (cm^2)	31.91	28.25	27.15	26.53	25.49

Table 8. The values of the joint displacements in the optimum single-layer Schwedler dome with $Nn = 8$ and $Nr = 3$.

Direction		x direction	y direction	z direction
	1	–	–	-2.76×10^{-2}
Joint no.	2	$+1.49 \times 10^{-3}$	-3.27×10^{-4}	-8.50×10^{-3}
	3	$+1.28 \times 10^{-3}$	$+8.22 \times 10^{-4}$	-8.50×10^{-3}

area is a big value. Obviously, the lowest volume is the one which has the smallest values, simultaneously, for the average cross-sectional area and the sum of the element lengths.

$$\bar{x} = \frac{\sum_{i=1}^{n} A}{n}. \tag{24}$$

From Table 9, related to the Schwedler domes with three rings, the optimum value for dome is obtained when Nn is set to 8 and 9. For the smaller values of Nn, as expected, the sections are very strong and, therefore, the average cross-sectional area becomes a higher value, and for the big values of Nn, the sum of the element lengths increases the volume of the dome. Similarly, from Table 6, for the domes with 4 rings with Nn as 6 and 7, economical designs are obtained. For the domes with 5 rings (Table 7), optimum values of Nn are 7 and 8. Accordingly, when Nn is constant, for example when it is 8, the sum of the element lengths in average for the Schwedler dome with 4 rings is 1.32 times larger than that for the dome with 3 rings. This value becomes 1.46 times larger when the domes with five and three rings are compared.

These differences are smaller when Nr remains constant and Nn is varied. As an example, the sums of the element lengths for the seven, eight, and nine nodes related to four-ring dome are 1.06, 1.12, and 1.18 times larger than that for the dome with six nodes on each ring, respectively. Therefore, as expected, when the number of rings changes, the alterations of $\bar{x}$ must be bigger than when the number of nodes is altered. In addition, the lowest value of $\bar{x}$ is found for the five-rings dome with 10 nodes on each ring, which is 25% and 5.5% percent lower than those for the domes with 4 rings and 3 rings with ten nodes on each ring, respectively. Therefore, in downward equipment loading condition, domes with the lowest volume have the weakest sections, and it does not depend on increasing Nn and/or Nr. As an example, for a dome with 5 rings and 7 nodes on each ring, we have stronger sections than the dome with four rings having the same Nr and Nn. These points are supported by the comparisons of the results made in Tables 6, 7, and 9. Also, according to Figure 8, the lowest volume is achieved when the dome is considered with 3 rings and 8 nodes. Under this load case, the optimum steel tubular designations for each member group obtained by the CBO algorithm, the height of the dome with different number of rings, and the max-

Table 9. Geometry and topology optimization of Schwedler domes with three rings using colliding bodies method.

Group number	$Nn = 6$	$Nn = 7$	$Nn = 8$	$Nn = 9$	$Nn = 10$
1	PIPST (10)	PIPST (10)	PIPST (10)	PIPST (10)	PIPST (10)
2	PIPST (10)	PIPST (6)	PIPST (5)	PIPST (5)	PIPST (5)
3	PIPST (8)	PIPST (6)	PIPST (5)	PIPST (5)	PIPST (5)
4	PIPST (3)	PIPST (3)	PIPST (3)	PIPST (3)	PIPST (3)
5	PIPST (5)	PIPST (2 1/2)	PIPST (1 1/2)	PIPST (1 1/2)	PIPST (1 1/2)
6	PIPST (8)	PIPST (8)	PIPST (8)	PIPST (8)	PIPST (8)
7	PIPST (4)	PIPST (4)	PIPST (3 1/2)	PIPST (3 1/2)	PIPST (3 1/2)
Height (m)	6.75	6.50	6.00	5.25	5.00
Max. displacement (cm)	2.75	2.78	2.76	2.79	2.70
Max. strength ratio	73.24	98.32	78.79	74.29	68.57
Volume	0.9331	0.7318	0.6833	0.7283	0.7784
$\sum l_I$ (m)	231.74	249.64	264.56	276.20	291.73
$\bar{x}$ (cm^2)	46.47	35.55	25.82	26.36	26.68

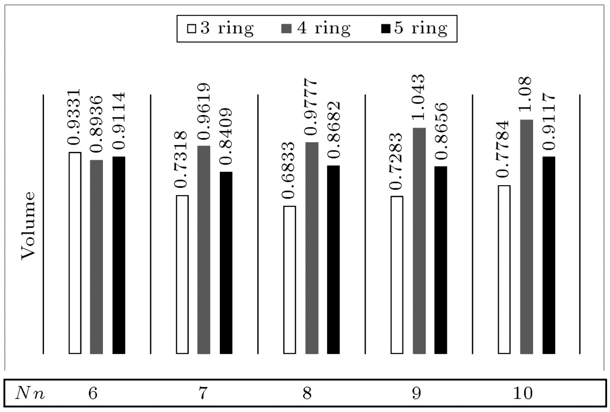

Figure 8. The volume comparison when Nn and Nr are varied.

Table 10. The values of the joint displacements in the optimum single-layer Schwedler dome with $Nn = 8$ and $Nr = 4$.

Direction		x direction	y direction	z direction
	1	–	–	-2.70×10^{-2}
Joint no.	2	$+5.56 \times 10^{-4}$	$+7.50 \times 10^{-4}$	-1.19×10^{-2}
	3	-1.37×10^{-4}	$+9.20 \times 10^{-4}$	-1.19×10^{-2}

imum values of restricted displacements by considering different number of nodes in each ring are given in Tables 6, 7, and 9 for Schwedler domes, respectively. The values of restricted displacement in the optimum domes obtained under downward equipment loading are shown in Tables 8, 10, and 11, respectively.

5.3. Optimum design of Schwedler dome under dead and snow loads

In this section, the dome described in the previous section is optimized using the CBO algorithm. In this case, the dead, snow, and lateral loads are considered

Table 11. The values of the joint displacements in the optimum single-layer Schwedler dome with $Nn = 8$ and $Nr = 4$.

Direction		x direction	y direction	z direction
	1	–	–	-2.79×10^{-2}
Joint no.	2	$+3.23 \times 10^{-4}$	$+7.40 \times 10^{-4}$	-1.59×10^{-2}
	3	-2.94×10^{-4}	$+7.52 \times 10^{-4}$	-1.59×10^{-2}

for Schwedler domes to investigate the real behavior and to obtain the optimum topology and geometry of the dome under these loading conditions.

The design dead load is established on the basis of the actual loads like the weight of various accessories and cladding that may be expected to act on the dome structure. The dead and snow loads are considered 200 N/m^2 and 800 N/m^2, respectively. The sum of dead and snow loads is computed as 1250 kN that is distributed between joints. Two horizontal loads in x and y directions are equal to 200 kN that are applied at the crown of dome as lateral loads.

At this stage, the number of rings is considered to be 3 under this loading condition. This number is chosen because according to the results of the previous section, the optimum number of rings for Schwedler dome is 3. The results of the design are shown in Table 12. Due to the existence of a noticeable value of dead/snow loading on each joint, the cross-sections are obtained close to each other. As can be seen, the optimum design of dome is found with 8 Nns on each ring. The dome with 6 number of nodes in each ring, because of having the least joints and simultaneously considerable load value on each joint, obtained almost higher volume for dome. Also, when the Nr is altered to 7 and Nn is changed to 8, the element lengths are increased, but the volume is decreased, because

Table 12. Optimum design of Schwedler under dead/snow loading ring using colliding bodies method.

Group number	$Nn = 6$	$Nn = 7$	$Nn = 8$	$Nn = 9$	$Nn = 10$
Group 1	PIPST (3 1/2)	PIPST (4)	PIPST (3 1/2)	PIPST (3 1/2)	PIPST (3 1/2)
Group 2	PIPST (3 1/2)	PIPST (4)	PIPST (3 1/2)	PIPST (3 1/2)	PIPST (3 1/2)
Group 3	PIPST (2 1/2)	PIPST (2)	PIPST (2)	PIPST (2)	PIPST (2)
Group 4	PIPST (2 1/2)	PIPST (2)	PIPST (1 1/2)	PIPST (1 1/2)	PIPST (2)
Group 5	PIPST (3 1/2)	PIPST (3 1/2)	PIPST (2 1/2)	PIPST (2 1/2)	PIPST (2)
Group 6	PIPST (2 1/2)	PIPST (3 1/2)	PIPST (3 1/2)	PIPST (3 1/2)	PIPST (3 1/2)
Group 7	PIPST (2 1/2)	PIPST (3 1/2)	PIPST (2 1/2)	PIPST (2 1/2)	PIPST (2 1/2)
Height (m))	8.00	7.25	6.75	6.00	5.50
Max. strength ratio	95.11	94.95	99.21	98.88	97.69
Volume	0.37	0.41	0.39	0.40	0.42
$\sum l_I$ (m)	241.04	255.99	271.56	283.44	296.88
$\bar{x}$ (cm^2)	15.70	16.38	14.11	14.11	14.18

the dead/snow load is distributed among more joints. For domes with 9 and 10 number of nodes in each ring, because of having considerable element length, the volume is increased again. From Table 12, it can be observed that a dome with small number of elements (Nn) tends to select greater height. When Nn decreases, the height of the dome increases, for a dome with small Nn, having a large height, helps the dome to prevent instability, as it was mentioned in the previous section. In short, a dome with 8 number of nodes in each ring has the optimum volume at this stage, which shows the lowest volume corresponding to the one which has the smallest values, simultaneously, for the average cross-sectional areas and the sum of the element lengths.

6. Concluding remarks

In this paper, the Colliding Bodies Optimization (CBO) and its enhanced version (ECBO) have been utilized for optimum design of Schwedler and ribbed domes. These algorithms determine the total number of rings, the number of nodes on each ring, the optimum height, and the optimum steel section designations for the members. CBO is inspired by the laws of collision between bodies. The governing laws from the physics initiate the base of CBO algorithm; each agent solution is considered to be a Colliding Body (CB). After the collision of two moving bodies, which has the specified mass and velocity, they separate with a new velocity. The main advantage of CBO is that unlike many other meta-heuristics, it is parameter-independent. From optimization point of view, CBO and ECBO provide a good balance between the exploration and the exploitation paradigms of the algorithm.

A complete investigation is performed on the effect of the number of rings and the number of nodes of the each ring on the final optimum design. Dead and snow load conditions are also taken into account. It is observed that the results obtained from these two algorithms are quite satisfactory and it is worthwhile to mention that ECBO has a better performance than CBO in terms of accuracy, reliability, and speed of convergence.

References

1. Fogel, L.J., Owens, A.J. and Walsh, M.J., *Artificial Intelligence Through Simulated Evolution*, Chichester, Wiley (1966).

2. Holland, J.H., *Adaptation in Natural and Artificial Systems*, Ann Arbor: University of Michigan Press (1975).

3. Eberhart, R.C. and Kennedy, J. "A new optimizer using particle swarm theory", In: *Proceedings of the Sixth International Symposium on Micro Machine and Human Science*. Nagoya, Japan (1995).

4. Dorigo, M., Maniezzo, V. and Colorni, A. "The ant system: Optimization by a colony of cooperating agents", *IEEE Transactions on System, Man and Cybernetics, Part B*, **26**(1), pp. 29-41 (1996).

5. Erol, O.K. and Eksin, I. "New optimization method: Big Bang-Big Crunch", *Advances in Engineering Software*, **37**, pp. 106-111 (2006).

6. Kaveh, A. and Talatahari, S. "A novel heuristic optimization method: Charged system search", *Acta Mechanica*, **213**, pp. 267-289 (2010).

7. Kaveh, A. and Khayatazad, M. "A novel meta-heuristic method: Ray optimization", *Computers and Structures*, **112-113**, pp. 283-294 (2012).

8. Kaveh, A. and Forhoudi, N. "A new optimization method: Dolphin echolocation", *Advances in Engineering Software*, **59**, pp. 53-70 (2013).

9. Kaveh, A. and Mahdavi, V.R. "Colliding bodiesoptimization: A novel meta-heuristic method", *Computers and Structures*, **39**, pp. 18-27 (2014).
10. Kaveh, A. and Talatahari, S. "Size optimization of space trusses using Big Bang-Big Crunch algorithm", *Computers and Structures*, **87**(17-18), pp. 1129-1140 (2009).
11. Saka, M.P. "Optimum geometry design of geodesic domes using harmony search algorithm", *Advances in Structural Engineering*, **10**(6), pp. 595-606 (2007).
12. Kaveh, A. and Talatahari, S. "Optimal design of Schwedler and ribbed domes via hybrid Big Bang-Big Crunch algorithm", *Journal of Constructional Steel Research*, **66**, pp. 412-419 (2010)
13. Kaveh, A. and Talatahari, S. "Optimal design of single layer domes using meta-heuristic algorithms; a comparative study", *International Journal of Space Structures*, **25**(4), pp. 217-227 (2010).
14. Kaveh, A. and Talatahari, S. "Geometry and topology optimization of geodesic domes using charged system search", *Structural Multidisciplinary Optimization*, **43**(2), pp. 215-229 (2011).
15. Gonçalves, M.S., Lopez, R.H. and Miguel, L.F.F. "Search group algorithm: A new metaheuristic method for the optimization of truss structures", *Computers and Structures*, **153**, pp. 165-184 (2015).
16. Mirjalili, S. "The ant lion optimizer", *Advances in Engineering Software*, **83**, pp. 80-98 (2015).
17. Taormina, R. and Chau, K.W. "Neural network river forecasting with multi-objective fully informed particle swarm optimization", *Journal of Hydroinformatics*, **17**(1), pp. 99-113 (2015).
18. Zhang, J. and Chau, K.W. "Multilayer ensemble pruning via novel multi-sub-swarm particle swarm optimization", *Journal of Universal Computer Science*, **15**(4), pp. 840-858 (2009).
19. Wang, W.C., Chau, K.W., Xu, D.M. and Chen, X.Y. "Improving forecasting accuracy of annual runoff time series using ARIMA based on EEMD decomposition",*Water Resource Management*, **29**(8), pp. 2655-2675 (2015).
20. American Institute of Steel Construction (AISC), *Manual of Steel Construction Allowable Stress Design*, 9th Ed., Chicago: AISC (1989).
21. Kaveh, A., *Advances in Metaheuristic Algorithms for Optimal Design of Structures*, Springer, Switzerland (2014).
22. Kaveh, A. and Ilchi Ghazaan, M. "Computer codes for colliding bodies optimization and its enhanced version", *International Journal of Optimization in Civil Engineering*, **4**(3), pp. 321-332 (2014).
23. Kaveh, A. and Ilchi Ghazaan, M. "Enhanced colliding bodies algorithm for truss optimization with dynamic constraints", *Journal of Computing in Civil Engineering, ASCE* (2014), 10.1061/ (ASCE) CP.1943-5487.0000445, 04014104.

Biographies

Ali Kaveh was born in 1948 in Tabriz, Iran. After graduation from the Department of Civil Engineering at the University of Tabriz in 1969, he continued his studies on Structures at Imperial College of Science and Technology at London University and received his MSc, DIC, and PhD degrees in 1970 and 1974, respectively. He then joined the Iran University of Science and Technology. Professor Kaveh is the author of 485 papers published in international journals and 135 papers presented at national and international conferences. He has authored 23 books in Farsi and 7 books in English, published by Wiley, RSP, and Springer.

Masoud Rezaei was born in 1991 in Khomein, Iran. He obtained his BSc degree in Civil Engineering from Shahid Rajaee Teacher Training University of Tehran in 2013, and at present he is MSc student in the Faculty of Earthquake Engineering at Road, Building, and Housing Research Center. His research interest is in optimum design of various types of dome structures.